International Conference of Agricultural Engineering
AgEng 2014 Zurich 6–10 July
Ref: C0xxx

Image registration for agricultural sensing tasks

Berenstein Ron, Ben-Gurion University of the Negev, Beer Sheva, Israel, berensti@bgu.ac.il

Ben-Shahar Ohad, Ben-Gurion University of the Negev, Beer Sheva, Israel, obs@cs.bgu.ac.il

Edan Yael, Ben-Gurion University of the Negev, Beer Sheva, Israel, yael@ bgu.ac.il

Godeša Tone, Agricultural Institute of Slovenia, Slovenia, tone.godesa@kis.si

Hočevar Marko, University of Ljubljana, Slovenia, marko.hocevar@fs.uni-lj.si

Abstract

Image registration is the process of overlaying two or more images of the same scene taken at different times, from different viewpoints, and/or by different sensors. This paper presents a method for automatic image registration for an agricultural spraying system that uses RGB and thermal cameras. The theoretical basis for creating a *Distance Dependent Transformation Matrix* (DDTM) is presented overcoming the complicated registration process caused by the fact that each sensor requires a different method to calculate its Control Points (CP).

Keywords: sensor registration, control points, artificial control points, sensor fusion

1 Introduction

This research is part of development of a selective robotic sprayer that aims to sense the tree foliage density and fruit position on the tree and to perform accurate spraying according to the detected target to reduce the amount of pesticides used. To provide accurate sensing the sprayer is equipped with three sensors: a thermal camera, a RGB camera and a laser distance scanner. Since the sensors have different features (e.g., spectral and spatial resolutions, distortions, fields of view, sensitivities) and are mounted at different locations (positions and orientations) on the sprayer, image registration is necessary to combine the image information.

Image registration is the process of overlaying two or more images of the same scene taken at different times, from different viewpoints, and/or by different sensors (Zitova and Flusser 2003). The process of image registration has been highly investigated (Brown and Steckler 1995, Zitova and Flusser 2003). Registration processes are usually divided into the following steps (Zitova and Flusser 2003); (**i**) Feature detection, known in the literature as Control Points (CP's). (**ii**) Feature matching. (**iii**) Transformation model estimation. (**iv**) Image resampling and transformation. The captured image is mapped according to the mapping functions.

Automatic image registration is needed for a robotic sprayer arm designed to work fully autonomously in a continuous operation mode. Automatic image registration is commonly used and is usually based on area based methods (methods that compare and match between the base image and the reference image without detecting features in the images,(Barnea and Silverman 1972, Pratt 1974, Althof et al. 1997) or feature based methods, methods that based the registration process on detecting the same CP's in the base image and the reference image (Stockman et al. 1982, Ton and Jain 1989, Lester and Arridge 1999, Zheng et al. 1999).

Applying automatic image registration on a system that uses visual and thermal images is extremely difficult due to the different methods employed to calculate the CP's for each type of sensor and the lack of correspondence between the CP's (Jarc et al. 2007).

The goal of this work is to introduce a new approach for high accuracy registration in field conditions while working with different thermal and RGB sensors when the distance between the object in the source image and the sensors is known. The registration approach is to create a Transformation Matrix (TM) in which each of the matrix elements is a function of the distance from the object in the image. The distance from the object was measured using a laser scanner.

2 Mathematical models

The core of the registration process is to find TM (equation 2.1) such that $\begin{bmatrix} x' \\ y' \end{bmatrix} = TM \cdot \begin{bmatrix} x \\ y \end{bmatrix}$, where x', y' is the registered pixel coordinates, x, y is the original pixel coordinates.

A projective transformation (Equation 2.5) was chosen due to its high number of DOF (8) which contribute to the registration accuracy (Szeliski 2010). Since the projective transformation matrix has 8 DOF, a linear system with size of at least 8 is required in order to determine a solution. From each independent CP two equations can be created while applying Equation 2.2 (Brown 1992 ENREF 3, Szeliski 2010) and all together at least four independent CP's are needed in order to create 8 linear independent equations. Increasing the number of CP's will contribute to better registration accuracy.

Equation 2.1

$$TM = \begin{bmatrix} h_{00} & h_{01} & h_{02} \\ h_{10} & h_{11} & h_{12} \\ h_{20} & h_{21} & h_{22} \end{bmatrix}$$

Equation 2.2

$$x' = \frac{h_{00}x + h_{01}y + h_{02}}{h_{20}x + h_{21}y + h_{22}} \qquad y' = \frac{h_{10}x + h_{11}y + h_{12}}{h_{20}x + h_{21}y + h_{22}}$$

Equation 2.3

$$A = \begin{bmatrix} x_1 & y_1 & 1 & 0 & 0 & 0 & -x_1'\cdot x_1 & -x_1'\cdot y_1 & -x_1' \\ 0 & 0 & 0 & x_1 & y_1 & 1 & -y_1'\cdot x_1 & -y_1'\cdot y_1 & -y_1' \\ & & & & & \vdots & & & \\ x_n & y_n & 1 & 0 & 0 & 0 & -x_n'\cdot x_n & -x_n'\cdot y_n & -x_n' \\ 0 & 0 & 0 & x_n & y_n & 1 & -y_n'\cdot x_n & -y_n'\cdot y_n & -y_n' \end{bmatrix}$$

The eigenvectors of the linear system (Equation 2.5) are calculated and according to the smallest eigenvalue, the eigenvector is then chosen for the TM.

A Distance Dependent Transformation Matrix (DDTM) ($TM(f(D))$) is dependent on distance D and it's constructing requires the following steps:

1. Capture a scenes with varying distances between the sensors and the target (the CP's) (Figure 2)
2. Calculate the TM for each scene
3. Construct a collection of all the TM calculated (Fig. 1)
4. Perform a linear regression on the TM's collection, for each matrix element separately (Equation 2.5)
5. Construct the DDTM (Equation 2.5)

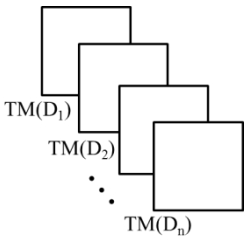

Fig. 1 - TM collection

Equation 2.4
$$DDTM\left(f(D)_{(m,n)}\right)=LR\left(TM(D_1)_{(m,n)},TM(D_2)_{(m,n)},\ldots,TM(D_n)_{(m,n)}\right)$$

Where Di is the distance between the target and the sensors, LR is Linear Regression, and (m,n) are the matrix element located at row m, column n.

Equation 2.5
$$DDTM\left(f(D)\right)=\begin{bmatrix} DDTM\left(f(D)_{(0,0)}\right) & DDTM\left(f(D)_{(0,1)}\right) & DDTM\left(f(D)_{(0,2)}\right) \\ DDTM\left(f(D)_{(1,0)}\right) & DDTM\left(f(D)_{(1,1)}\right) & DDTM\left(f(D)_{(1,2)}\right) \\ DDTM\left(f(D)_{(2,0)}\right) & DDTM\left(f(D)_{(2,1)}\right) & DDTM\left(f(D)_{(2,2)}\right) \end{bmatrix}$$

Using Equation 2.5 as the TM, each pixel new coordinates will be calculated according to its distance D.

3 Artificial control points

A unique Artificial Control Points (ACP) chart was designed with the goal to be easily detected by the two sprayer imagery sensors, the RGB camera and the thermal camera. The ACP is assembled from two elements, a colored disk (120mm diameter) with 10[W] light bulb fixed at the disk center (Figure 1a). The disks were colored differently in order to increase the correspondence between the detected ACP on the RGB image and the thermal image. The colored disk detection algorithm was based on color filtration (according to the specific disk) and the light bulb detection algorithm was based on temperature value filtration. Both algorithms included morphological operations.

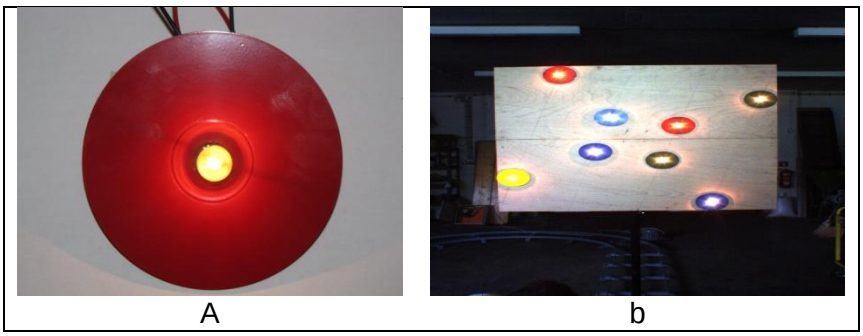

Figure 1 - ACP's. (a) single target with a 10W light bulb in the middle, (b) flat plate with 8 CP targets

In order to calculate a reliable DDTM in a real world scene, eight ACP's were mounted to a flat plate (1x1[m]) according to Fig. 5a. The plate dimensions and the ACP's arrangement within the plate were chosen such that at the minimum operational distance between the plate and the sensors array (170cm) the ACP's will cover most of the image area (Fig. 5b). Covering most of the image area with CP's will contribute to the DDTM robustness since the model will take into account more image disturbance exists in the image surroundings. The ACP's flat plate was mounted to the rail-cart with the ability to move while the plate remains perpendicular to the sensors array.

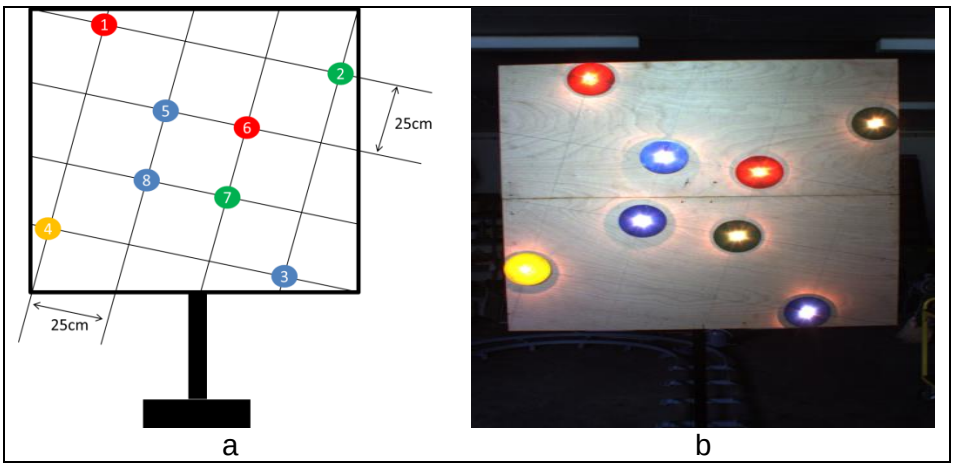

Figure 2 - ACP's arrangement (a) and sample RGB image of ACP's mounted on a plate.

4 Experiments

Two experiments were performed. The first experiment was performed to create the transformation matrix. The second experiment was conducted in order to validate the registration process.

4.1 Experimental setup - target rail and sensor position

The experimental system included two main elements: sensor array (Figure 1a) and a circular rail with mobile rail-cart (Figure 1b)**.** The sensor array contained three sensors, RGB camera (Flea2 FL2-08S2C with resolution of 768X1032 and 45° wide angle lens), thermal camera (Flir T425 with resolution of 240X320 and 45° IR wide angle lens), and laser scanner (Sick LMS111 with scanning angle of 270° and resolution of 0.5°). The sensors were mounted to the sprayer disabling any relative movement among sensors during all experiments. The second experiment element is a circular rail (width 6.4 m \ length 2.4 m) with a mobile rail-cart (Figure 1b) able to move along the rail line. The rail-cart position\velocity can be controlled manually or by using an AC driver (frequency controller). Several types of targets can be fixed on top of the rail-cart such as artificial targets or real-world target (live trees).
Data from all three sensors was acquired simultaneously using a personal computer and stored for later analysis.

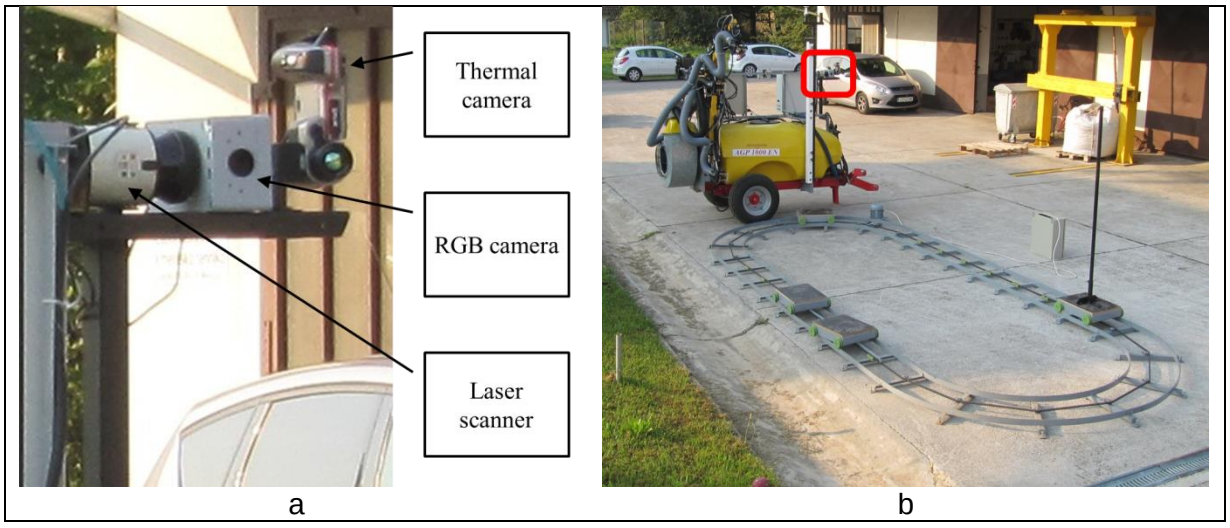

Figure 3 - Selective sprayer. (a) sensors array, (b) overall sprayer with rail (red square, sprayer sensors)

4.2 First experiment – distance dependent transformation matrix creation

The first experiment goal is to create the $DDTM(f(D))$. Creating the DDTM requires sampling of TM from several distances and performing linear regression on the results.

4.2.1 Experimental setup

In order to calculate the $DDTM(f(D))$, 51 scenes were captured from distances varying from 1700 to 3450 [mm] between the sensor array and the ACP's plate with intervals of 50 [mm] resulting in a total of 37 distances. These distances correspond to the operational distances of the specific sprayer system. Each captured scene includes a single visual image from the RGB camera, a single thermal image and a single laser scan that includes the plate surface.

4.2.2 DDTM calculation

Acquiring the ACP's positions from the visual image (Figure 4a) is mainly performed by color filtration and morphological operations to remove image noise resulting in a binary image (Figure 4b) that contains solely the ACP's objects. The ACP position for the visual image (Figure 4c) is calculated as the mass center of each ACP object.

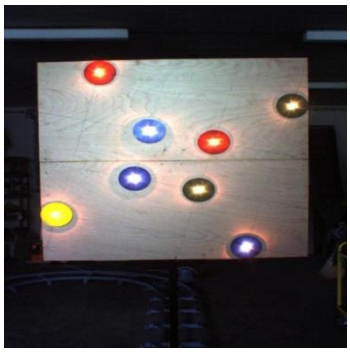

a

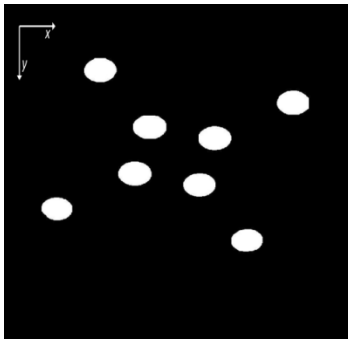

b

Num	*X*	*Y*
1	215.3361	204.0696
2	645.5506	304.7588
3	542.6099	728.1052
4	118.8685	630.5358
5	325.7399	379.1956
6	470.7419	413.5364
7	436.6628	557.197
8	292.6094	522.4266

c

Figure 4 – (a) Visual image, (b) RGB ACP's positions, (c) ACP's position (sort according to Figure 2a)

Since the temperature of the light bulb positioned at the disk center is significantly higher than all background objects, acquiring the ACP's positions from the thermal image (Figure 5a) is solely performed by value (temperature) filtration. Filtration of the thermal image results with a binary image (Figure 5b) that contains solely the ACP's objects. The mass center of each ACP object is calculated and the resulting coordinate is considered to be the ACP position for the thermal image (Figure 5c).

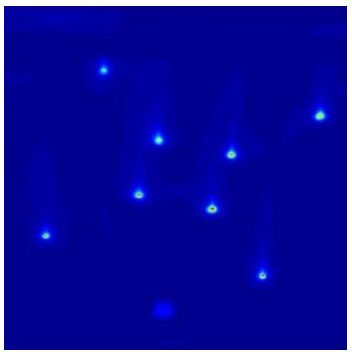

a

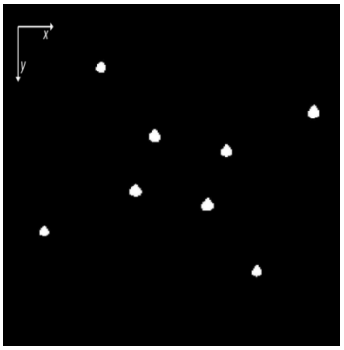

b

Num	*X*	*Y*
1	70.20755	59.86792
2	221.5867	101.76
3	181.1111	250.3148
4	29.83673	213.1224
5	108.4865	124.1216
6	159.5588	138.0588
7	146.0513	188.4103
8	94.82432	175.2297

c

Figure 5 - (a) Thermal image, (b) Thermal ACP's position, (c) ACP's position (numbers according to Figure 2a)

A projective TM was calculated for mapping the visual image to the thermal image, according to the mathematical model, for each of the 51 scenes for all the distances between the sensors and the plate. Averaging the 51 TMs for each distance provides a reliable TM for the given distance.

Linear regression was used for all the TM elements except for h_{02} where third degree polynomial regression was used.
The $DDTM(f(D))$ calculated shown in (Equation 1):

Equation 1

$$DDTM(f(D)) = \begin{bmatrix} 0.3729 & -0.0135 & -2\cdot10^{-9}D^3 + 2\cdot10^{-5}D^2 - 0.0695D + 70.047 \\ 0.0231 & 0.3632 & -0.0003D - 17.957 \\ 0 & 0 & 1 \end{bmatrix}$$

4.3 Second experiment – DDTM validation

Validation of the DDTM was established using the calculated ACP's positions. The visual ACP's were mapped to the thermal ACP's using the calculated $DDTM(f(D))$. Since the goal was to map the RGB image to the thermal image, the pixel distance between each mapped RGB ACP and the thermal ACP represents the registration error.
The registration error was calculated for all the images (51 in total) from all distances (1700~3450). Figure 6 summarizes the registration error at different distances.

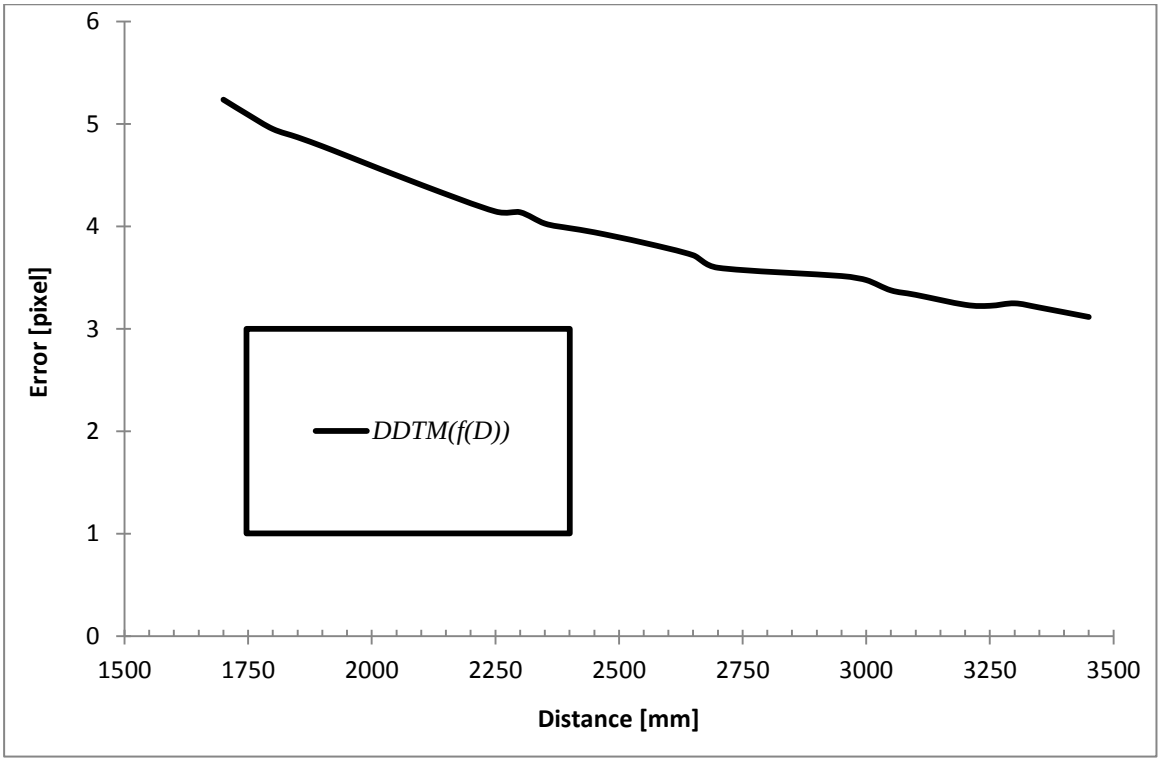

Figure 6 – registration error [pixels]

5 Conclusions and future work

The results show that the maximum error for the registration was ~5 [pixel]. Although this error is acceptable for agricultural use, future work will concentrate on minimizing this error.
These promising results show that this registration method can be used for applications that require several sensors of different types.
Future ongoing work includes error and sensitivity analyses and experiments with angled planes and vibrating targets.

6 Acknowledgements

This research was funded by the European Commission in the 7th Framework Programme (CROPS GA no. 246252) and partially supported by the ABC Robotics Center funded by

Helmsley Charitable Trust and by the Rabbi W. Gunther Plaut Chair in Manufacturing Engineering, both at Ben-Gurion University of the Negev.

7 References

Althof, R. J., M. G. J. Wind and J. T. Dobbins III (1997). A rapid and automatic image registration algorithm with subpixel accuracy. Medical Imaging, IEEE Transactions on 16(3): 308-316.

Barnea, D. I. and H. F. Silverman (1972). A class of algorithms for fast digital image registration. Computers, IEEE Transactions on 100(2): 179-186.

Brown, L. G. (1992). A survey of image registration techniques. ACM computing surveys (CSUR) 24(4): 325-376.

Brown, R. B. and J. Steckler (1995). Prescription maps for spatially variable herbicide application in no-till corn. Trans. of the ASAE 38(1): 1659-1666.

Jarc, A., J. Pers, P. Rogelj, M. Perse and S. Kovacic (Year) of Conference. Texture features for affine registration of thermal (FLIR) and visible images. Computer Vision Winter Workshop, Citeseer.

Lester, H. and S. R. Arridge (1999). A survey of hierarchical non-linear medical image registration. Pattern recognition 32(1): 129-149.

Pratt, W. K. (1974). Correlation techniques of image registration. Aerospace and Electronic Systems, IEEE Transactions on(3): 353-358.

Stockman, G., S. Kopstein and S. Benett (1982). Matching images to models for registration and object detection via clustering. Pattern Analysis and Machine Intelligence, IEEE Transactions on(3): 229-241.

Szeliski, R. (2010). Computer vision: Algorithms and applications, Springer.

Ton, J. and A. K. Jain (1989). Registering Landsat images by point matching. Geoscience and Remote Sensing, IEEE Transactions on 27(5): 642-651.

Zheng, Z., H. Wang and E. Khwang Teoh (1999). Analysis of gray level corner detection. Pattern Recognition Letters 20(2): 149-162.

Zitova, B. and J. Flusser (2003). Image registration methods: a survey. Image and vision computing 21(11): 977-1000.